Polymer 135 (2018) 305–313

Contents lists available at ScienceDirect

Polymer

journal homepage: www.elsevier.com/locate/polymer

Performance of high lignin content cellulose nanocrystals in poly(lactic acid)

Liqing Wei [a], Umesh P. Agarwal [a], Laurent Matuana [b], Ronald C. Sabo [a, **], Nicole M. Stark [a, *]

[a] USDA Forest Service, Forest Products Laboratory, Madison, WI 53726, United States
[b] School of Packaging, Michigan State University, East Lansing, MI 48824, United States

ARTICLE INFO

Article history:
Received 28 September 2017
Received in revised form
1 December 2017
Accepted 12 December 2017
Available online 13 December 2017

Keywords:
Cellulose nanocrystals
Nanolignin
Hydrothermally-treated wood
Interface
Nanocomposites
Poly(lactic acid)

ABSTRACT

High lignin-containing cellulose nanocrystals (HLCNCs) were successfully isolated from hydrothermally treated aspen fibers and freeze-dried and compounded with poly (lactic acid) (PLA) by extrusion and injection molding. As a comparison, PLA composites containing commercial lignin-coated CNCs (BLCNCs) were also produced. HLCNCs showed higher crystallinity, larger surface area, lower degree of agglomeration, and more hydrophobic surfaces compared to BLCNCs, as characterized by electron microscopy, surface area measurements, thermal analysis, spectroscopy and water contact angle measurements. The effect of lignin and CNC morphology on the mechanical, thermal and viscoelastic properties and CNCs/polymer interfacial adhesion of nanocomposites was investigated with tensile test, DSC and DMA. Compared to neat PLA, the Young's modulus, elongation to break, and toughness of PLA/2%HLCNCs were improved by 14, 77, and 30%, respectively. HLCNCs and BLCNCs act as nucleating fillers, increasing the degree of crystallinity (χ_c) of PLA in nanocomposites. The presence of lignin nanoparticles in the HLCNC increased the compatibility/adhesion between CNCs and polymer matrix which increased the storage modulus.

Published by Elsevier Ltd.

1. Introduction

Using cellulose nanocrystals (CNCs) as renewable reinforcing agent or biofiller for polymeric composites has attracted academia and industrial interest for its high specific surface area, crystallinity and modulus [1,2]. Currently, CNCs are mainly produced by acid hydrolysis of cellulose from lignin-free (bleached) wood or plant fibers. However, CNCs are destined for high hydrophilicity due to the large number of hydroxyl groups on their surfaces, which leads to poor interaction and compatibility between CNCs and hydrophobic polymer matrices [2–4]. In addition, in most cases, the CNCs are produced as aqueous suspensions because of their hydrophilic nature, resulting in agglomerate during drying [5]. This is dramatically compromising the dispersion of dried CNCs in a polymer matrix.

Lignin, another major component of plant/woody biomass, has relatively higher surface polarity/hydrophobicity than cellulose. Lignin molecules can embed themselves between cellulose chains to hinder hydrogen bonds, and therefore less agglomeration is expected compared with lignin-free nanocellulose. Lignin has great UV-absorption capability, hence, the nanocellulose containing lignin with a dualfunctional UV-absorbing and reinforcing fillers in composites. This advantage would pave the way of lignin-containing nanocellulose to be potentially applied for UV-blocking food packaging materials [6,7].

Several studies have been attempted to produce cellulose nanofibrils (CNFs) from unbleached fibers containing lignin, hemicelluloses and extractives [1]. However, these studies have mostly focused on the economic perspectives and nanopaper applications of the lignin-containing CNFs (LCNFs). Gupta et al. [8] reported that the commercial grade lignin-coated CNCs (America Process Inc.) was able to improve the processability and thermophysical properties of resulting PLA based nanocomposites. However, no publications are available that address the precise effect of lignin hydrophobicity on the interfacial bonding and performance of lignin-containing CNCs (or CNFs) in nanocellulose polymer composites. In a publication by Agarwal et al. [9], it was reported that never-dried native wood cellulose is not crystalline and CNCs

* Corresponding author.
** Corresponding author.
E-mail addresses: rsabo@fs.fed.us (R.C. Sabo), nstark@fs.fed.us (N.M. Stark).

https://doi.org/10.1016/j.polymer.2017.12.039
0032-3861/Published by Elsevier Ltd.

could not be produced from untreated wood by the commonly used 64% H_2SO_4 hydrolysis process. In other words, it has been the various pulping processes that contribute to the formation of crystalline region in cellulose and therefore, in CNCs and CNFs. These authors further reported that crystallization of wood cellulose occurred upon hydrothermal treatment of wood and CNCs (both lignin-containing and lignin-free) could be produced from the thermally treated aspen [9,10].

In this study, hydrothermally-treated aspen wood fibers were selected as the feedstock for cellulose nanocrystals production. No delignification/bleaching process was performed on the treated aspen fibers; hence, the resulting CNCs are lignin-containing CNCs. These CNCs (HLCNCs) were freeze-dried, and they, as well as commercial grade spray-dried lignin-coated CNCs (BLCNCs), were compounded with PLA. The chemical composition, morphology, thermal stability, surface chemistry, crystalline structure and surface hydrophobicity of the two types of CNCs were characterized and compared. The injection molded nanocomposites were evaluated for their mechanical, thermal, and viscoelastic properties. Interfacial adhesion between the HLCNCs (or BLCNCs) and the polymer matrix was elucidated. Thus, this work reports a systematic investigation of the effect of lignin on the CNCs role as a filling/reinforcing agent for polymer composites.

2. Experimental

2.1. Materials

PLA pellets (Ingeo™, 4044D) were obtained from NatureWorks LLC (Minnetonka, MN, US) [11]. The density of PLA pellets was 1.24 g/cm^3. PLA pellets were Wiley milled into <40 mesh powder. During the milling process, PLA pellets and the mill were kept cold by liquid nitrogen to avoid PLA degradation/melting. PLA powder was dried for overnight in a vacuum oven at ambient temperature prior to melt processing.

The high lignin-containing CNCs were derived from hydrothermally treated aspen wood fibers followed by a typical CNCs production process by sulfuric acid hydrolysis [12]. Briefly, the aspen fibers were placed in a Berghof reactor vessel reactor that was sealed. The ramp time was 75min and the vessel was held at 170 °C for 90min. The treatment was quenched by placing the reactor vessel in a cold-water bath. The treated wood and solution were filtered through a sintered glass funnel and were washed with RO water until the filtrate was almost colorless. The wet filter cake was air dried and then hydrolyzed with 64% sulfuric acid to produce the high lignin-containing CNCs (HLCNCs) suspension, following the conventional CNCs production procedure that has been developed at USDA Forest Products Laboratory (Madison, WI, USA) [12,13]. The HLCNCs suspension was then quickly frozen in liquid nitrogen, followed by freeze-drying process for 3 days to obtain the dry HLCNCs. The morphology of the HLCNCs before and after drying were evaluated by transmission electron microscopy (TEM) and scanning electron microscopy (SEM) [12].

BLCNCs in powder form (under the trade name of Bioplus-L® Crystal) was purchased from American Process Inc. (Atlanta, USA) as a comparison [14]. These BLCNCs were produced by first fractionating biomass into cellulose, hemicelluloses and lignin using proprietary pulping processes, and then dissolved lignin was precipitated onto cellulose surfaces followed by mechanical treatment and finally spray-drying [14]. The chemical composition analysis was conducted on HLCNCs and BLCNCs according to the method described elsewhere [15]. As shown in Table 1, the commercial BLCNCs contain about 19% xylan whereas it was hardly present in HLCNCs, indicating the hemicelluloses was removed during the hydrothermal treatment and upon hydrolysis by the 64% H_2SO_4. At 49%, the lignin content of HLCNCs was four times of that for BLCNCs. This is because the sulfuric acid can only dissolve acid soluble lignin and some cellulose, resulting in a substantially enriched lignin in the HLCNCs.

Table 1
Chemical composition of lignin-coated and lignin-containing CNCs (as % dry weight).

Sample	Glucan	Xylan	Mannan	Klason lignin	Ash
HLCNCs	51.4	0.2	Not detected	48.6	0.2
BLCNCs	70.4	18.7	0.3	10.2	0.3

2.2. Nanocomposites processing

Ten grams total of PLA powder and CNCs (0.5, 1, 2, and 5 wt%) were premixed manually in a beaker and then fed into a microprocessing co-rotating twin screw extruder (DSM Xplore 15 mL, DSM Research, The Netherlands). Zones 1, 2, and 3 were set at 175, 180, and 185 °C, screw speed was 100 rpm and cycle time was 2 min. The extrudates were collected and injection molded into Type V tensile or rectangular specimens (69 mm × 12.6 mm × 3.2 mm) using DSM Xplore 12 mL microinjection molding machine at 185 °C. Mold temperature, pressure, and processing time were 105 °C, 8 bars, and 30s, respectively. The samples were designated as neat PLA, PLA/0.5%HLCNC, PLA/1% HLCNC, PLA/2%HLCNC, PLA/5%HLCNC, PLA/0.5%BLCNC, PLA/1% BLCNC, PLA/2%BLCNC, and PLA/5%BLCNC, representing nanocomposites made from 0.5, 1, 2, and 5% of BLCNCs and/or HLCNCs.

2.3. Characterization

2.3.1. Fourier transform infrared (FTIR) analysis

FTIR spectra of HLCNCs and BLCNCs were recorded using a Thermo Nicolet iZ10 spectrometer equipped with an ATR probe. Spectra were recorded using a spectral width ranging from 4000 to 600 cm^{-1}, with 4 cm^{-1} resolution and an accumulation of 128 scans.

2.3.2. Thermogravimetric analysis (TGA)

TGA was performed under nitrogen flow (20 mL/min) from 50 to 700 °C at the heating rate of 10 °C/min using a Perkin Elmer Pyris 1.0 analyzer [16,17].

2.3.3. Wide-angle X-ray diffraction (WAXD)

WAXD experiments of CNCs were carried out at room temperature on powdered CNC samples with a D8 Discover diffractometer (Bruker AXS Inc., USA) by irradiating the HLCNCs and BLCNCs with Cu Kα radiation. The operating conditions are i) accelerating voltage of 50 kV and current of 1000 μA, ii) rotating Cu Kα X-ray IMS tube, and iii) $2\theta = 5–60°$ with 0.005°/s. The peak intensities of the crystalline and amorphous diffractions were measured after peak fitting using Gaussian function in IGOR software. The crystallinity index of CNCs (HLCNCs and BLCNCs) was calculated according the Segal's method [17,18]:

$$CrI\% = (1- (I_{am}/I_{002})) \times 100 \quad (1)$$

where I_{am} and I_{002} represent the intensity of amorphous and the (002) plane diffraction.

2.3.4. Contact angle measurements

The dynamic contact angle of sessile drops of water on the nanocrystals was measured with an Attention Theta Lite Optical

Tensiometer (KSV Instrument Ltd., Finland). Detailed sample preparation can be found in our previous research [17]. All measurements were conducted from 0 to 10s. As a comparison, the contact angle of lignin (dealkaline, TCI Chemicals, Japan) was measured following the same procedure as CNCs.

2.3.5. BET analysis

The specific surface area of the BLCNCs and HLCNCs samples (0.10 g, in duplicate) was determined by N_2 adsorption using a TriStar II plus analyzer (Micromeritics Instrument Corp.). Before analysis the sample was vacuum degassed for 12 h at 25 °C followed by 2 h at 150 °C. N_2 isotherms were collected at 77 K and a partial pressure range of 0.001–0.99, within this range 88 absorption points were specified. BET analysis was used to determine the apparent surface area (SA) from the N_2 isotherm using data from points collected at partial pressure between 0.001 and 0.1 [19]. Total pore volume (V_T) was determined from the maximum adsorption quantity at a partial pressure of approximately 0.99 for the N_2 isotherm.

2.3.6. Tensile testing

The tensile test of injection molded nanocomposites was conducted at 23 °C and 50% relative humidity using an Instron 5865 system (Instron Engineering Corp., MA, USA) equipped with a 500 N load cell. ASTM D standard 638-02 was followed with following modifications, a 7.68 mm gauge length was used and the tests were performed with a crosshead speed of 1 mm/min. The strain was measured using a LX 500 laser extensometer (MTS systems Corp., MN, USA) with sampling frequency of 10 Hz. The tensile strength (σ) was taken as the maximum stress level. The data were fit to a hyperbolic tangent in order to determine the Young's modulus (E) by taking slope of the fitted stress-strain curve at the initial linear region. Elongation to break (ε, %) was recorded at failure. Ten specimens were tested for each sample. The density (ρ, g/cm^3) of injection molded rectangular samples (5 replicates) was calculated from the initially conditioned dry weight and dimensions. The fractured surfaces, after tensile test, were coated with a thin layer of gold and examined using SEM.

2.3.7. Dynamic mechanical analysis (DMA)

DMA of the injection molded nanocomposites rectangular bars in the 3-point bending mode was performed on TA Q800 (TA Instrument, New Castle, DE, USA). The measurements were carried out at a constant frequency of 1 Hz, strain amplitude of 0.5%, a temperature range from 25 to 130 °C, and at a heating rate of 2 °C/min. Three specimens were tested to validate the results.

The nanocrystals/matrix interface was further evaluated by using the adhesion factor (A) which was determined from the damping versus temperature [3,20,21]:

$$A = (1/(1\text{-}V_r)) \times (\tan\delta_c/\tan\delta_m - 1) \quad (2)$$

where c and m subscripts represent nanocomposites and matrix, and the V_r is the CNC volume fraction, which was determined as follows:

$$V_r = (W_r\rho_m)/(W_r\rho_m + W_m\rho_r) \times 100 \quad (3)$$

where W_r is weight of CNCs, W_m is the weight of matrix, ρ_r is the density of CNCs ($\rho_r = 1.59$ g/cm^3), and ρ_m is the density of PLA ($\rho_m = 1.24$ g/cm^3) [22,23]. Calculated V_r values of nanocomposites, containing 0.5, 1, 2, and 5 wt% CNCs, were 0.4, 0.8, 1.6, and 3.9%, respectively.

2.3.8. Differential scanning calorimetry (DSC)

DSC tests were conducted using a TA Instrument Q2000 differential scanning calorimeter equipped with a refrigerated cooling system. Sample (4 mg) was placed and sealed in Tzero aluminum pans and tested under continuous N_2 flow (50 mL/min). Each sample was heated from 40 to 190 °C at a heating rate of 10 °C/min, kept at this temperature for 5min, and then cooled down at a cooling rate of 10 °C/min and isothermally kept for 5min, finally followed by the second heating scan at 10 °C/min to 190 °C. Melting temperature (T_m), cold crystallization temperature (T_{cc}), and enthalpies (ΔH_m and ΔH_{cc}) were determined from the second heating curve. The degree of crystallinity (χ_c) of PLA was calculated as follows [3,24]:

$$\chi_c\% = \Delta Hm/(\Delta H_m{}^0 - \Delta H_{cc})/W_{PLA} \times 100 \quad (4)$$

where ΔH_m is the enthalpy the melting peak, $\Delta H_m{}^0$ is enthalpy in J/g of 100% crystalline PLA (93.6 J/g) [11], ΔH_{cc} is the cold crystallization enthalpy, and W_{PLA} is the wt% of PLA in composites.

2.3.9. Statistical analysis

Significance in the differences of density, tensile properties and adhesion factors were statistically analyzed using one-way analysis of variance (ANOVA) by software R version 3.2.2 (The R Foundation, https://www.r-project.org/) at an α level of 0.05 employing a Tukey's test.

3. Results and discussion

3.1. Morphology and surface area of CNCs

The hydrothermal treatment followed by acid hydrolysis results in elongated nanocrystals (HLCNCs) with higher aspect ratio. The rod-like HLCNCs exhibit an average diameter (d) of 10 ± 1 nm and a length (L) of about 134 ± 7 nm as estimated by TEM (Fig. 1). The aspect ratio (L/d = 13) [13,23], which is higher than that of the conventional lignin-free CNCs (SCNCs: L/d = 8) derived from dissolving pulp using the similar sulfuric acid hydrolysis as for HLCNCs. In addition, lignin nanoparticles (or nanolignin, the ball-shape particles) with diameter of 2–22 nm are produced during the HLCNC production process, as observed in Fig. 1.

During the dehydration of high lignin-contained CNCs water suspensions, complete replacement of the water by tert-butanol during solvent exchange stage was difficult to achieve [5]. This

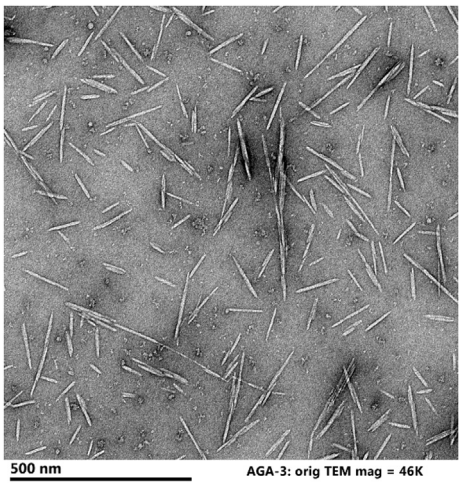

Fig. 1. Transmission electron micrograph of high lignin-containing CNCs before drying.

can further result in CNC agglomeration/aggregation due to the three-dimensional hydrogen bonding formed between CNC molecules, while water is evaporated during the freeze-drying process [1,17,25]. As seen in the micrographs of Fig. 2a, micro-scale HLCNC aggregated particles were observed. However, the size of the agglomers was much smaller than the freeze-dried lignin-free CNCs that were reported in our previous research [17]. Some HLCNCs flakes have smooth surfaces (Fig. 2b) while some are more porous with nano-scaled particles (nano-rods) present on the large aggregated surfaces (Fig. 2c). The porous surface structure of HLCNCs may be helpful in the polymer melt attachment and thereby, better CNCs/polymer interfacial bonding could be accomplished. The BLCNCs showed agglomerates with size ranging from 1 to 50 μm and large rod-like particles were present (Fig. 2d, e, and 2f), which agrees well with studies reported previously [8].

In order to quantitatively characterize surface area (SA) and porosity of HLCNCs and BLCNCs, the former was determined by BET analysis. The SA of HLCNCs was $29.3 \pm 0.2\ m^2/g$, which is more than twenty times of the SA for BLCNCs ($1.9 \pm 0.1\ m^2/g$). Note this is close to value of $1.29\ m^2/g$ reported previously for general spray-dried lignin-free CNCs [26]. This is likely contributed to the lignin nanoparticles (or nanolignin), CNCs nano-rods and porous structure which was observed in freeze-dried HLCNCs, as indicated in the SEM images (Fig. 2c). Moreover, during the freeze-drying process, the presence of relatively more hydrophobic lignin could hinder the hydrogen-bonding formation between cellulose surface chains of the CNCs. Nevertheless, the SA values of both CNCs were significantly lower than the theoretical values for typical CNCs (e.g. $419\ m^2/g$ [27]). This confirms that the large agglomerates with dimensions in the range of micron to hundreds of microns are formed during drying; thus, lower accessible surface areas are created. The total volume (V_T) of freeze-dried HLCNCs was $0.046 \pm 0.003\ m^3/g$, and much of the pore volume was located within mesopores (2–25 nm) with an average particle size of 205 nm, whereas the V_T of BLCNCs was 0.004 ± 0.000 with an average size of 3089 nm. This agrees with SA result, which was significantly lower for BLCNCs.

3.2. Thermal stability of CNCs

The thermogravimetric (TG) and derivative thermogravimetric (DTG) curves of BLCNCs and HLCNCs are shown in Fig. 3. The onset temperature (T_{onset}) of starting-to-degradation for HLCNCs and BLCNCs is about 305 °C. The temperature of maximum degradation rate (T_{max}) of sample BLCNCs was 54 °C higher than of HLCNCs (332 °C). It is worth noting that HLCNCs were prepared via sulfuric acid hydrolysis to break down the cellulose non-crystalline domains, which is the similar production mechanism for lignin-free CNCs. The sulfate groups are introduced onto the surface of HLCNCs by esterification during hydrolysis and a rapid reduction in its degree of polymerization is due to the presence of sulfate groups. It is known that the CNCs with sulfate groups degrade at lower temperature compared to their non-sulfated counterparts [28]. About 63% of HLCNCs and 76% of the BLCNCs was degraded at $T \leq 500$ °C due to the degradation of cellulose and lignin. Considering the DTG curve, the HLCNC show two distinctive stages,

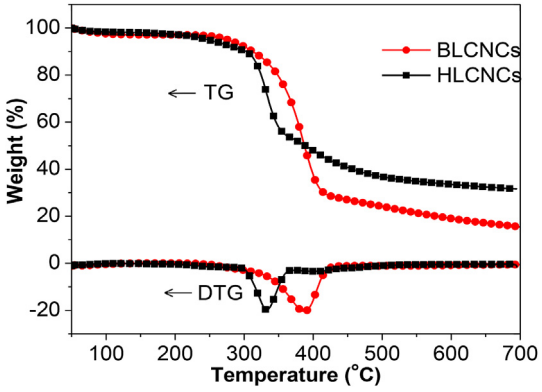

Fig. 3. TG and DTG curves of nanocrystals.

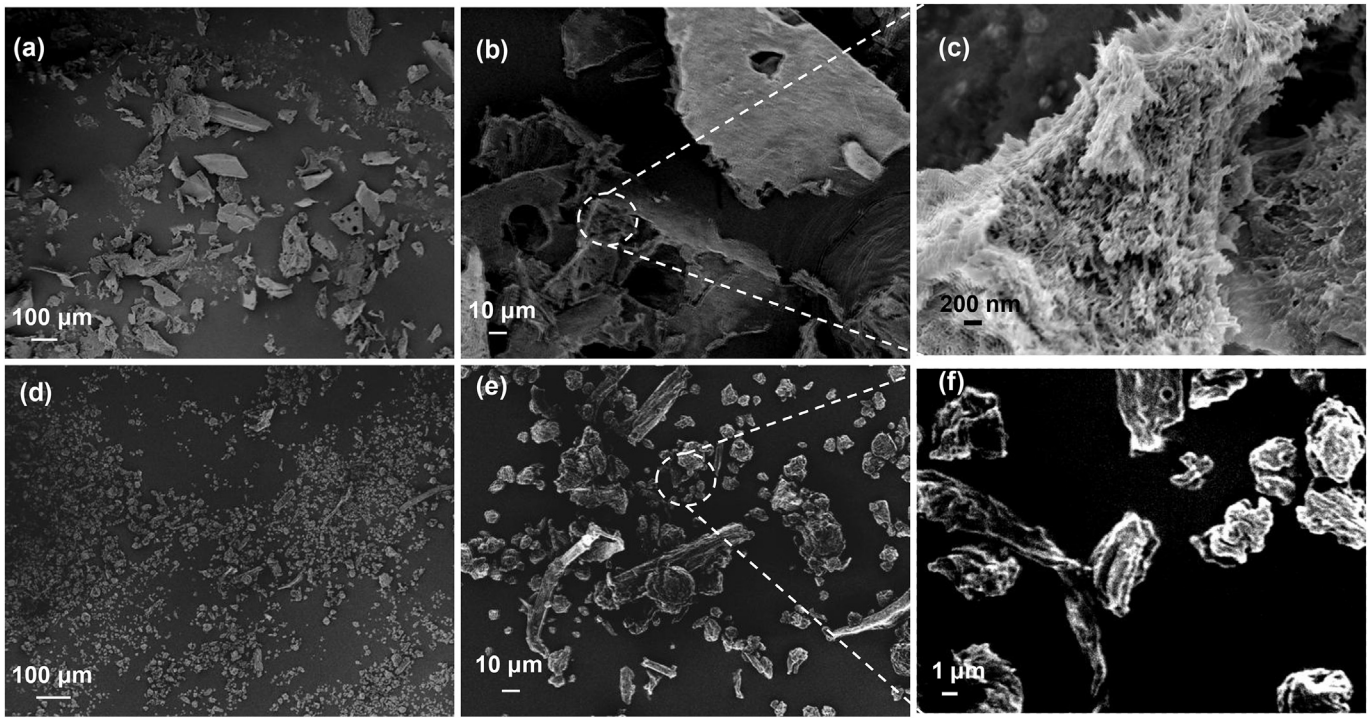

Fig. 2. Morphologies of the freeze-dried HLCNCs (a–c) and spray-dried BLCNCs (*d*–f).

(i) < 360 °C and (ii) 360–500 °C. Stage (i) is ascribed to the degradation of HLCNCs, while stage (ii) could mostly be due to degradation of lignin including nanolignin. The char residual yield at 700 °C was about 31% and 15% of the original weight of the HLCNCs and BLCNCs, respectively, and the higher amount attributed to the higher lignin content of HLCNCs. The 5% weight reduction of HLCNCs and BLCNCs occurs at 248 °C and 272 °C which are much higher than the compounding and injection molding temperatures for the nanocomposites in this study (<190 °C). Though HLCNCs have slightly lower thermal stability than BLCNCs, the degradation temperature is significantly higher than most polymer melt processing temperatures (<260 °C). Hence, the thermal stability cannot be considered as a disadvantage if used for polymer composites.

3.3. Surface chemistry and crystalline structure of CNCs

As shown in Fig. 4a, FTIR spectra confirmed the chemical nature of lignin-containing and lignin-coated CNCs (HLCNCs and BLCNCs, respectively). Apparent fingerprint peaks of lignin at 1515 cm^{-1} and 1606 cm^{-1} were observed in HLCNCs, whereas these peaks showed much lower intensity for BLCNCs (Fig. 4a). In non-phenolic spectral region, for BLCNCs, a peak was observed at 1735 cm^{-1} (C=O vibration), indicating the presence of xylan (Fig. 4a). No corresponding detectable C=O vibration was observed in HLCNCs, confirming that xylan was hydrolyzed and washed away during the CNC production process which is also supported by the chemical analysis data reported in Table 1. These findings are also in a good agreement with the chemical compositional analysis (Table 1).

X-ray diffraction patterns of the freeze-dried HLCNCs and spray-dried BLCNCs are given in Fig. 4b. HLCNCs and BLCNCs have an average CrI% of 89.6 ± 1.0 and 81.6 ± 2.0 based on three replicate measurements, which are higher than CrI% of lignin-free CNCs (SCNCs) that were produced from bleached eucalyptus kraft pulp by sulfuric acid hydrolysis [29,30]. The higher CrI% of the CNCs used here may explain their higher thermal stability compared to SCNCs (T_{onset} = 218 °C; CrI% = 77.9). Higher CrI% of HLCNCs is likely to arise due to the hydrothermal treatment of aspen fibers before CNCs production process [9,10].

3.4. Surface hydrophobicity of CNCs

Compared to cellulose, lignin has more hydrophobic surface due to the relatively lower O/C ratio [31]. Here, because both HLCNCs and BLCNCs contain lignin, they are expected to be more hydrophobic compared to conventional CNCs produced from bleached kraft pulp or dissolving pulp. Since the ultimate goal of this study is to demonstrate the high lignin-containing CNCs are suitable as biofiller into a hydrophobic polymer matrix, contact angles (CA) were used to estimate the hydrophobicity of CNC surfaces (Table 2). The average CA for HLCNCs (69°) was much higher than that for lignin (50°) and BLCNCs (50°). The lignin surface showed water droplet spreading with time as compared to the BLCNCs and HLCNCs. The results indicated that the HLCNCs surface is significantly more hydrophobic, thus better interfacial bonding between HLCNCs and hydrophobic polymer matrix is expected, which will be discussed later as adhesion factor.

3.5. Mechanical properties of nanocomposites

Densities and mechanical tensile properties were evaluated for PLA filled with HLCNCs and BLCNCs for different compositions are shown in Table 3. Because the densities of all types of nanocomposites are statistically the same to that of neat PLA, in the following, only the absolute tensile properties rather than the specific tensile properties are reported and discussed. Compared to PLA, improvements in Young's modulus (E) and strain at break (ε, %) after 0.5% addition of HLCNCs and beyond, and after 1% addition of BLCNCs and beyond. Neat PLA is considered to be a brittle polymer, not able to deform much (ε = 7.4%). Hence, the addition of both HLCNCs and BLCNCs results in more ductile nanocomposites. The effect of HLCNCs on tensile strength (σ) of composites was not significant (Table 3). No improvement of σ of composites as a consequence of filler agglomeration. However, dramatic decrease of σ was reported previously for the freeze-dried lignin-free CNCs and PLA nanocomposites [32,33]. Upon comparison of the mechanical properties between PLA/BLCNCs and PLA/HLCNCs, the latter

Table 2
Water contact angle as a function of contact duration.

Time (s)	Contact angle (°)			
	HLCNCs	BLCNCs	Lignin	PLA
0	73.2 ± 1.4	53.6 ± 3.4	61.1 ± 4.2	88.8
0.5	71.7 ± 1.0	52.5 ± 3.0	56.7 ± 4.3	88.7
1	69.6 ± 0.4	51.7 ± 2.9	54.1 ± 3.6	88.8
2	68.9 ± 0.1	50.6 ± 3.3	49.0 ± 5.6	88.8
5	65.1 ± 1.4	48.4 ± 3.1	43.3 ± 4.3	88.8
10	64.0 ± 1.2	45.3 ± 3.1	34.9 ± 2.6	88.6
Average	68.7 ± 0.8	50.4 ± 2.9	49.8 ± 4.0	88.8

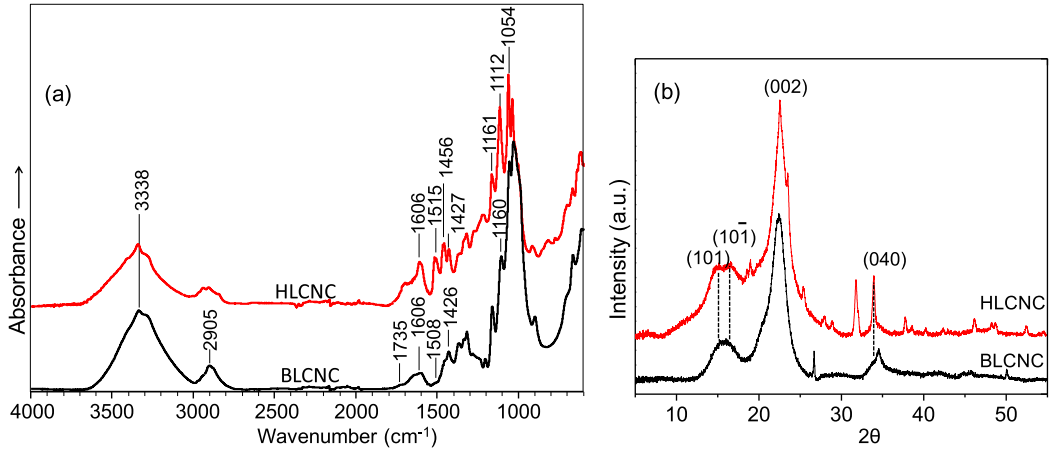

Fig. 4. (a) FTIR spectra and (b) WAXD diffractograms of BLCNCs and HLCNCs.

Table 3
Density (ρ) and mechanical properties of PLA and nanocomposites as determined by tensile testing (Young's modulus (E), ultimate strength (σ) and elongation to break (ε)).[a]

Sample	ρ (g/cm^3)	E (GPa)	σ (MPa)	ε (%)	U_T (MJ/m^3)
PLA	1.24 (0.1)^a	3.7 (0.6)^a	64.4 (2.3)^a	7.1 (1.2)^a	2.0 (0.1)^a
PLA/0.5%HLNC	1.10 (0.0)^a	4.3 (0.5)^b	61.2 (2.8)^{ab}	11.4 (1.5)^b	2.3 (0.1)^a
PLA/1%HLNC	1.09 (0.0)^a	4.2 (0.4)^b	63.4 (3.0)^{ac}	11.6 (1.2)^b	2.7 (0.2)^b
PLA/2%HLNC	1.18 (0.0)^a	4.2 (0.4)^b	62.9 (3.0)^{ac}	12.6 (1.2)^b	2.6 (0.1)^b
PLA/5%HLNC	1.06 (0.1)^a	4.5 (0.5)^b	59.4 (2.3)^{ac}	11.3 (2.1)^b	1.3 (0.1)^c
PLA/0.5%BLNC	1.20 (0.1)^a	4.1 (0.2)^a	60.3 (1.2)^{bd}	8.2 (0.7)^a	1.1 (0.1)^c
PLA/1%BLNC	1.12 (0.1)^a	4.8 (0.9)^b	58.4 (2.5)^{bd}	12.3 (1.2)^b	1.5 (0.2)^c
PLA/2%BLNC	1.12 (0.1)^a	4.8 (0.6)^b	58.2 (3.5)^{bd}	11.6 (1.2)^b	1.3 (0.1)^c
PLA/5%BLNC	1.13 (0.1)^a	4.6 (0.7)^b	55.7 (2.6)^c	11.0 (1.3)^b	0.6 (0.1)^d

[a] Variations are given in parentheses. Samples with different letters are significantly different at 95% confidence interval of probability according to Tukey's paired t-tests.

nanocomposites showed higher tensile strength than the former nanocomposites (Table 3) [15]. Hence, these tensile testing results led to the conclusion that HLCNCs have better adhesion to the polymer matrix compared to BLCNCs. This indicated there is better stress-transfer at the HLCNCs/PLA interface, which is supported by the water contact angle results (Table 2) that the HLCNCs surface is more hydrophobic than BLCNCs. Additionally, toughness (U_T) of materials was estimated by integrating the area under the stress-strain curves. A significant increase in toughness was realized with the addition of 1, 2, and 5% HLCNCs. That was not the case with BLCNCs (Table 3). For example, compared to U_T of 2.0 MJ/m^3 of neat PLA, the U_T of PLA/2%HLNC increased to 2.6 MJ/m^3, an increase of 30%. This suggested reinforcing/toughening effect of nanolignin in PLA may be due to the similarity in solubility parameter of lignin (22–23.5MPa$^{1/2}$) [34] and PLA (23.1MPa$^{1/2}$) [35]. However, when the content of HLCNCs and BLCNCs was increased from 2% to 5%, no additional increase of U_T was obtained, which is again probably due to the aggregates of freeze-dried HLCNCs and spray-dried BLCNCs. Hence, it can be concluded that the mechanical properties of nanocomposites are not improved when HLCNCs/BLCNCs content is increased to 5%.

After the tensile testing, fractured surfaces for neat PLA, PLA/2% HLCNC, and PLA/2%BLCNC were examined by SEM. As shown in Fig. 5, compared with the smooth surface of PLA (Fig. 5a), HLCNCs (Fig. 5b) and BLCNCs (Fig. 5c) can be seen in the nanocomposites. Composites surface showed microfibrilation ascribed to the ductile deformation, which agrees to the tensile results, higher elongation. These ductile fibrils surrounding the HLCNCs appear to bridge the gaps/voids at the polymer-HLCNCs interface. Large HLCNCs agglomerates can be observed in PLA/2%HLCNC (Fig. 5b), which presumably lead to stress concentration at the surfaces of the large agglomerates and contributes to the poorer performance of tensile strength as expected. Both apparent voids and microductility phenomena were observed at the fractured surfaces of PLA/2% BLCNC. This suggested some competing factors resulting in reduced tensile strength but improved ductility (ε) and stiffness (E).

3.6. Thermal properties

The effect of adding HLCNCs or BLCNCs on the crystallization and melting behavior of composites was studied by DSC, and the results are reported in Table 4. Glass transition (T_g) was not influenced by the incorporation of HLCNCs or BLCNCs into PLA. This likely indicated that the relatively small amount and large sizes of CNCs are not sufficient to change the polymer chain mobility within the glass transition region. In the current study, the degree of crystallinity (χ_c) was found to have increased by adding either HLCNCs or BLCNCs, because CNCs perform as a nucleating agent for PLA composites and facilitates PLA crystallization [36]. When the CNCs concentrations were increased from 2 to 5%, the χ_c was reduced slightly. This is likely to be due to relatively poorer dispersion of CNCs into the polymer matrix and the higher fraction of large agglomerates, which slightly inhibited the nucleation effect of CNCs. It is interesting to see double melting peaks (T_{m1} and T_{m2}, representing peaks from low to high temperature) of the PLA/HLCNCs composites. It is speculated that there could be two types of crystalline structures present in the PLA/HLCNCs nanocomposites [37]. The lower-temperature endotherm might be attributed to the melting of original PLA crystals, while the one at higher temperature could be caused by the melting of the secondary crystallization resulting from the rearrangement of the crystallizable amorphous polymer segments around the nanolignin particles. This further confirmed the higher cold crystallization enthalpies, ΔH_{cc} (J/g), of the PLA/HLCNCs as compared with neat PLA and corresponding PLA/BLCNCs systems.

3.7. Viscoelastic properties by DMA

DMA is a useful technique to study the relationship between the structure and viscoelastic behavior of polymer and polymer-fiber composites. For nanocomposites, the storage modulus (E′) and damping factor (tanδ) are shown in Fig. 6 as a function of temperature. For the temperature of below T_g, the storage modulus,

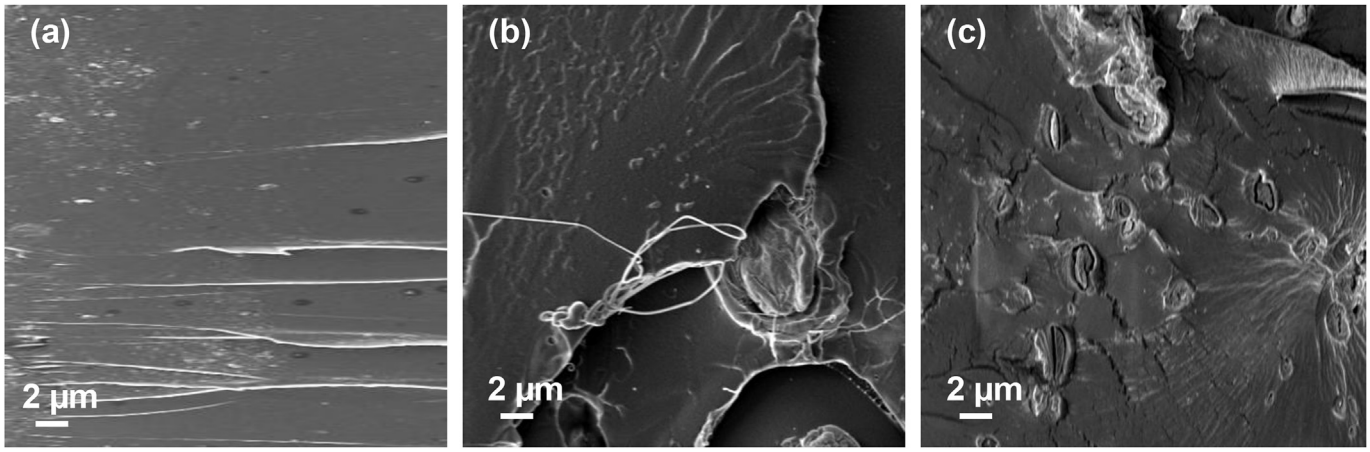

Fig. 5. SEM images of fractured surfaces after tensile testing: (a) PLA, (b) PLA/2%HLCNCs and (c) PLA/2%BLCNCs.

Table 4
Thermal properties of PLA and composites from the second heating scan by DSC.

Sample	T_g (°C)	T_{cc} (°C)	ΔH_{cc} (J/g)	T_m (°C)	ΔH_m (J/g)	χ_c (%)
PLA	60.8	117.4	18.1	149.0	22.2	4.4
PLA/0.5%HLCNC	60.6	115.8	14.9	147.8 (T_{m1}), 154 (T_{m2})	23.2	8.9
PLA/1%HLCNC	60.4	115.6	20.4	147.7 (T_{m1}), 154 (T_{m2})	27.0	7.1
PLA/2%HLCNC	60.9	115.2	20.3	148.0 (T_{m1}), 154 (T_{m2})	25.0	5.1
PLA/5%HLCNC	60.6	115.0	21.8	147.7(T_{m1}), 154 (T_{m2})	26.2	4.9
PLA/0.5%BLCNC	60.8	115.8	14.5	148.4	25.0	11.3
PLA/1%BLCNC	60.6	115.2	14.2	147.7	23.9	10.5
PLA/2%BLCNC	59.8	115.3	14.4	147.6	23.1	9.5
PLA/5%BLCNC	60.1	114.8	17.0	147.3	24.0	7.9

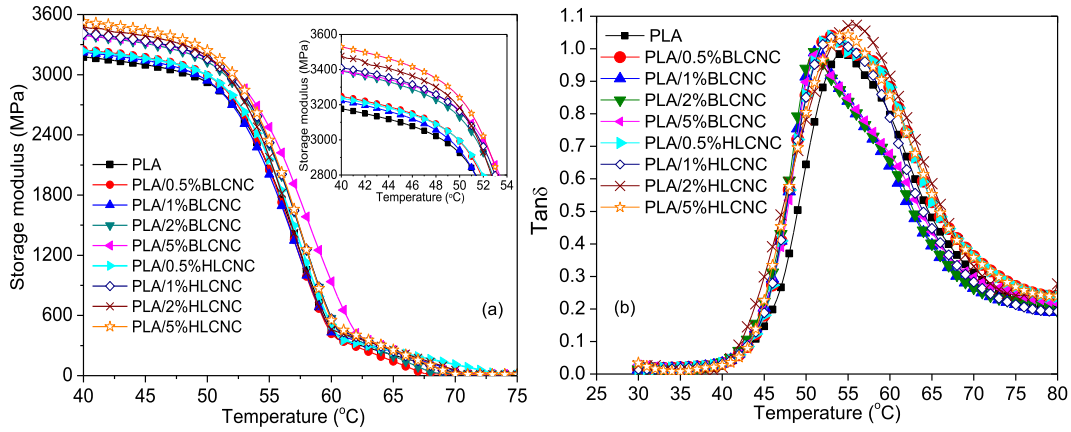

Fig. 6. Storage modulus (a) and Tan δ (b) versus temperature for neat PLA and nanocomposites.

reflecting the dynamic rigidity for all samples, decreased slightly with temperature but remained almost stable (Fig. 6a). The significant reduction was observed when sample entered into glass rubber transition stage, which can be attributed to softening of the polymer due to increase in the polymer chain slippage at high temperatures. The nanocomposites exhibited higher storage modulus compared to neat PLA, especially in the glassy region, showing the potential as reinforcement, especially for HLCNCs. Similar results have been reported in nanocomposites that were filled with BLCNCs [8]. The intensity of tanδ peak for neat PLA was higher than all the nanocomposites. This can be attributed to the confinement effect of CNCs, reduced chain mobility of the composite materials, and energy/stress loss due to inter-friction between the molecular chains in the amorphous region of polymer matrix. The glass transition temperature can be defined as the temperature where the inflection points corresponding to a significant drop in the E′ or the tanδ is maximum. The T_g of PLA obtained from E' (Fig. 6a) and tanδ (Fig. 6b) plots was about 54 °C, which is slightly lower than the value from DSC analysis ($T_g = 60.8$ °C). The tanδ values of nanocomposites, containing 1, 2 and 5% of BLCNCs, showed a dramatic drop when temperature was higher than the tanδ peak temperature (often referred as glass transition temperature, T_g). This is possibly caused by the slippage of polymer chains due to relatively poorer interaction of polymer matrix and BLCNCs. On the other hand, good interaction between HLCNCs and PLA was noted due to the broadening of tanδ peak and increases in T_g of PLA/HLCNCs nanocomposites. Similar findings were reported for polybutylene succinate (PBS) and lignin composites [38]. The major cause of the increase in T_g for PLA/HLCNCs may be the creation of an amorphous region component in composites where the polymer and HLCNCs are closely associated, resulting the reduced free volume of the nanocomposites.

In order to evaluate the interfacial adhesion between the CNCs and PLA matrix, the adhesion factor (*A*) was calculated from DMA results according to Equations (2) and (3), and the results are summarized in Table 5. It has been demonstrated that the lower *A* values indicate higher degree of interfacial interaction at the fill/polymer interface [3,20,21]. Adhesion factor values were averaged from the temperature range between 28 and 55 °C, because most properties are determined below glass transition temperature (60 °C) and most PLA based biocomposites are used in packaging, agricultural and horticulture applications (e.g., yogurt cups, trays and bowls for fast food, and mulching films) close to room temperatures [39]. All the *A* results are summarized in Table 5. All *A* values for PLA/HLCNC are lower than those for PLA/BLCNC, indicating better interfacial adhesion between the HLCNC and the polymer matrix. As an example, for *A* calculation of sample PLA/2% BLCNC, the average $\tan\delta_c/\tan\delta_m$ near to room temperature is about 1.13, while the V_f of PLA/2%BLCNC is 3.9%. Hence, to plug these

Table 5
CNC volume fractions (V_f) and adhesion factor (*A*) values for nanocomposites.[a]

Sample	W_f (%)	V_f (%)	Adhesion factor (*A*)
PLA	0	0.0	–
PLA/0.5%HLNC	0.5	0.4	0.211[a]
PLA/1%HLNC	1	0.8	0.184[a]
PLA/2%HLNC	2	1.6	0.142[a]
PLA/5%HLNC	5	3.9	0.119[b]
PLA/0.5%BLNC	0.5	0.4	0.230[c]
PLA/1%BLNC	1	0.8	0.221[b]
PLA/2%BLNC	2	1.6	0.178[b]
PLA/5%BLNC	5	3.9	0.158[d]

[a] Samples with same letter are not significantly different at 95% confidence interval of probability using Tukey paired t-tests.

values into Eq. (2), *A* was 0.179. Adhesion factors agree well with the storage modulus results that lower *A* values were obtained for nanocomposites (PLA/5%HLCNC, PLA/2%HLCNC, PLA/5%BLCNC, PLA/2%BLCNC, and PLA/1%HLCNC) also had higher storage moduli for these five formulations. Among the nanocomposites, the PLA/5% HLCNC had the best interfacial interaction (lowest *A*) between CNCs and the polymer matrix. The results explained why the static and dynamic mechanical properties were improved by adding HLCNCs.

4. Conclusions

Conventional CNCs are mostly produced from lignin-free wood-pulps and large agglomerations are formed during various drying process, resulting in poor adhesion at the CNCs/polymer interface and dispersion of CNCs within the polymer matrix. Herein, laboratory produced high lignin-containing and commercial lignin-coated CNCs (HLCNCs and BLCNCs, respectively) were used to produce PLA/CNCs nanocomposites. HLCNCs produced by acid hydrolysis of thermally treated wood showed attractive characteristics as a filler/reinforcing material for PLA/CNCs composites and outperformed the commercial spray-dried CNCs (BLCNCs). Compared to conventional lignin-free CNCs derived from sulfuric acid hydrolysis of bleached pulp, the HLCNCs-based composites had higher thermal stability, higher crystallinity, more hydrophobic surfaces, lower degree of agglomeration and higher surface area. The addition of HLCNCs increased the toughness of resulting composites compared to neat PLA polymer. Incorporation of either BLCNCs or HLCNCs resulted in significantly improvements in both Young's modulus and elongation to break but small decreases in tensile strength. When the BLCNCs (or HLCNCs) was increased from 2 to 5%, no additional increase was observed in Young's modulus. Similarly, the PLA degree of crystallinity (χ_c%) was increased for both BLCNCs and HLCNCs. Dynamic mechanical analysis showed that the storage modulus of the nanocomposites was increased by adding CNCs, especially by HLCNCs. Broader peak of tanδ indicated the better interaction between HLCNCs and polymer matrix. It can be concluded that the HLCNCs derived from hydrothermally-treated wood can be used as excellent filler and/or reinforcing agents to improve the physical and thermal properties for polymer nanocomposites. However, approaches for improved dispersion of cellulose nanomaterials in PLA are still needed.

Acknowledgements

The authors acknowledge the Public-Private Partnership for Nanotechnology (P^3Nano) US Endowment for Forestry and Communities, Inc. The authors would like to thank the following people from USDA Forest Service, Forest Products Laboratory: Sally A. Ralph for preparing hydrothermally treated wood fiber, Richard S. Reiner for preparing the lignin-free freeze-dried CNCs, Dr. Samuel L. Zelinka and Charles R. Boardman for the help with DSC, Jane O'Dell for the kind technical guidance to DMA experiments, Dr. J.Y. Zhu and Huiyang Bian for water contact angle measurements, Dr. Craig Clemons for the daily inspired discussions, Neil Gribbins and Philip Walsh for the help with Wiley mill and TGA instrumentation, and Sara Fishwild, Tim Nelson and Marshall Begel for assistance in tensile test and date analysis.

References

[1] R.J. Moon, S. Beck, A.W. Rudie, Cellulose nanocrystals – a material with unique properties and many potential applications, in: M.T. Postek, R.J. Moon, A.W. Rudie, M.A. Bilodeau (Eds.), Production and Applications of Cellulose Nanomaterials, TAPPI Press, Peachtree Corners, GA, 2013, pp. 9–12.
[2] L. Wei, A. McDonald, A review on grafting of biofibers for biocomposites materials 9 (4) (2016) 303, https://doi.org/10.3390/ma9040303.
[3] L. Wei, N.M. Stark, A.G. McDonald, Interfacial improvements in biocomposites based on poly(3-hydroxybutyrate) and poly(3-hydroxybutyrate-co-3-hydroxyvalerate) bioplastics reinforced and grafted with α-cellulose fibers, Green Chem. 17 (10) (2015) 4800–4814.
[4] L. Wei, A.G. McDonald, N.M. Stark, Grafting of bacterial polyhydroxybutyrate (PHB) onto cellulose via in situ reactive extrusion with dicumyl peroxide, Biomacromolecules 16 (3) (2015) 1040–1049.
[5] Y. Peng, D.J. Gardner, Y. Han, Drying cellulose nanofibrils: in search of a suitable method, Cellulose 19 (1) (2011) 91–102.
[6] J.A. Sirvi, M. Visanko, J.P. Heiskanen, H. Liimatainen, UV-absorbing cellulose nanocrystals as functional reinforcing fillers in polymer nanocomposite films, J. Mater. Chem. 4 (17) (2016) 6368–6375.
[7] W. Yang, E. Fortunati, F. Dominici, G. Giovanale, A. Mazzaglia, G.M. Balestra, J.M. Kenny, D. Puglia, Effect of cellulose and lignin on disintegration, antimicrobial and antioxidant properties of PLA active films, Int. J. Biol. Macromol. 89 (2016) 360–368.
[8] A. Gupta, W. Simmons, G.T. Schueneman, D. Hylton, E.A. Mintz, Rheological and thermo-mechanical properties of poly(lactic acid)/lignin-coated cellulose nanocrystal composites, ACS Sustainable Chemistry & Engineering 5 (2) (2017) 1711–1720.
[9] U.P. Agarwal, S.A. Ralph, R.S. Reiner, C. Baez, Probing crystallinity of never-dried wood cellulose with Raman spectroscopy, Cellulose 23 (1) (2015) 125–144.
[10] U.P. Agarwal, S.A. Ralph, R.S. Reiner, C. Baez, Production of cellulose nanocrystals from raw wood via hydrothermal treatment. Patent pending, Application serial no. 15/455211, USPTO, 2017.
[11] L. Wei, S. Luo, A.G. McDonald, U.P. Agarwal, K.C. Hirth, L.M. Matuana, R.C. Sabo, N.M. Stark, Preparation and characterization of the nanocomposites from chemically modified nanocellulose and poly (lactic acid). https://doi.org/10.7569/JRM.2017.634144, 2017. Journal of Renewable Materials.
[12] L. Wei, U. Agarwal, N. Stark, R. Sabo, Nanocomposites from Lignin-containing Cellulose Nanocrystals and Poly(lactic Acid), ANTEC 2017, Society of Plastics Engineers, Anaheim, CA, USA, 2017.
[13] R. Reiner, A. Rudie, Process Scale-Up of Cellulose Nanocrystal Production to 25 kg per Batch at the Forest Products Laboratory, in: M.T. Postek, R.J. Moon, A.W. Rudie, M.A. Bilodeau (Eds.), Production and Applications of Cellulose Nanomaterials, TAPPI Press, Peachtree Corners, GA, 2013, pp. 21–24.
[14] K. Nelson, T. Retsina, Innovative nanocellulose process breaks the cost barrier, TAPPI 13 (2014) 19–23.
[15] S. Liang, A.G. McDonald, Chemical and thermal characterization of potato peel waste and its fermentation residue as potential resources for biofuel and bioproducts production, J. Agric. Food Chem. 62 (33) (2014) 8421–8429.
[16] H. Xu, F. Tong, J. Yu, L. Wen, J. Zhang, J. He, A one-pot method to prepare transparent poly (methyl methacrylate)/montmorillonite nanocomposites using imidazolium-based ionic liquids, Polym. Int. 61 (9) (2012) 1382–1388.
[17] L. Wei, U.P. Agarwal, K.C. Hirth, L.M. Matuana, R.C. Sabo, N.M. Stark, Chemical modification of nanocellulose with canola oil fatty acid methyl ester, Carbohydr. Polym. 169 (2017) 108–116.
[18] L. Segal, J.J. Creely, A.E. Martin, C.M. Conrad, An empirical method for estimating the degree of crystallinity of native cellulose using the x-ray diffractometer, Textil. Res. J. 29 (10) (1959) 786–794.
[19] L. Wei, S. Liang, N.M. Guho, A.J. Hanson, M.W. Smith, M. Garcia-Perez, A.G. McDonald, Production and characterization of bio-oil and biochar from the pyrolysis of residual bacterial biomass from a polyhydroxyalkanoate production process, J. Anal. Appl. Pyrol. 115 (2015) 268–278.
[20] L. Wei, S. Liang, A.G. McDonald, Thermophysical properties and biodegradation behavior of green composites made from polyhydroxybutyrate and potato peel waste fermentation residue, Ind. Crop. Prod. 69 (2015) 91–103.
[21] L. Wei, A.G. McDonald, C. Freitag, J.J. Morrell, Effects of wood fiber esterification on properties, weatherability and biodurability of wood plastic composites, Polym. Degrad. Stabil. 98 (7) (2013) 1348–1361.
[22] J.H. Lee, S.H. Park, S.H. Kim, Preparation of cellulose nanowhiskers and their reinforcing effect in polylactide, Macromol. Res. 21 (11) (2013) 1218–1225.
[23] X. Xu, F. Liu, L. Jiang, J.Y. Zhu, D. Haagenson, D.P. Wiesenborn, Cellulose nanocrystals vs. Cellulose nanofibrils: a comparative study on their microstructures and effects as polymer reinforcing agents, ACS Appl. Mater. Interfaces 5 (8) (2013) 2999–3009.
[24] L. Wei, A.G. McDonald, Peroxide induced cross-linking by reactive melt processing of two biopolyesters: poly(3-hydroxybutyrate) and poly(L-lactic acid) improve their melting processability, J. Appl. Polym. Sci. 132 (2014) 41724, https://doi.org/10.1002/app.41724.
[25] J. Peng, P.J. Walsh, R.C. Sabo, L.-S. Turng, C.M. Clemons, Water-assisted compounding of cellulose nanocrystals into polyamide 6 for use as a nucleating agent for microcellular foaming, Polymer 84 (2016) 158–166.
[26] A. Brinkmann, M. Chen, M. Couillard, Z.J. Jakubek, T. Leng, L.J. Johnston, Correlating cellulose nanocrystal particle size and surface area, Langmuir 32 (24) (2016) 6105–6114.
[27] L. Heath, W. Thielemans, Cellulose nanowhisker aerogels, Green Chem. 12 (8) (2010) 1448.
[28] N. Wang, E. Ding, R. Cheng, Thermal degradation behaviors of spherical cellulose nanocrystals with sulfate groups, Polymer 48 (12) (2007) 3486–3493.
[29] L. Chen, Q. Wang, K. Hirth, C. Baez, U.P. Agarwal, J.Y. Zhu, Tailoring the yield and characteristics of wood cellulose nanocrystals (CNC) using concentrated acid hydrolysis, Cellulose 22 (3) (2015) 1753–1762.
[30] L. Chen, J.Y. Zhu, C. Baez, P. Kitin, T. Elder, Highly thermal-stable and

functional cellulose nanocrystals and nanofibrils produced using fully recyclable organic acids, Green Chem. 18 (13) (2016) 3835–3843.
[31] Å. Henriksson, P. Gatenholm, Surface properties of CTMP fibers modified with xylans, Cellulose 9 (2002) 55–64.
[32] N. Herrera, A.M. Salaberria, A.P. Mathew, K. Oksman, Plasticized polylactic acid nanocomposite films with cellulose and chitin nanocrystals prepared using extrusion and compression molding with two cooling rates: effects on mechanical, thermal and optical properties, Compos. Appl. Sci. Manuf. 83 (2016) 89–97.
[33] L. Wei, N.M. Stark, R.C. Sabo, L. Matuana, Modification of cellulose nanocrystals (CNCs) for use in poly(lactic acid) (PLA)-CNC composite packaging Products, in: Proceedings, Forest Products Society International Convention, June 28-29, 2016. Portland, OR.
[34] W. Thielemans, R.P. Wool, Lignin esters for use in unsaturated thermosets: lignin modification and solubility modeling, Biomacromolecules 6 (2005) 1895–1905.
[35] I. Pillin, N. Montrelay, Y. Grohens, Thermo-mechanical characterization of plasticized PLA: is the miscibility the only significant factor? Polymer 47 (13) (2006) 4676–4682.
[36] E. Sullivan, R. Moon, K. Kalaitzidou, Processing and characterization of cellulose nanocrystals/polylactic acid nanocomposite films, Materials 8 (12) (2015) 8106–8116.
[37] O. Martin, L. Avérous, Poly(lactic acid): plasticization and properties of biodegradable multiphase systems, Polymer 42 (14) (2001) 6209–6219.
[38] S. Sahoo, M. Misra, A.K. Mohanty, Enhanced properties of lignin-based biodegradable polymer composites using injection moulding process, Compos. Appl. Sci. Manuf. 42 (11) (2011) 1710–1718.
[39] M. Jamshidian, E.A. Tehrany, M. Imran, M. Jacquot, S. Desobry, Poly-lactic acid: production, applications, nanocomposites, and release studies, Compr. Rev. Food Sci. Food Saf. 9 (5) (2010) 552–571.